Attitude Stabilization of a Micro-Aerial Vehicle with Sliding Mode Control

Joe Mockler
Department of Aerospace Engineering
University of Maryland, College Park
College Park, MD
jmockle1@umd.edu

***Abstract*—This work attempts to control a nonlinear micro-aerial vehicle (MAV) using sliding mode control. The MAV dynamics are first introduced in a complete sense, then through assumptions and results from previous system identification work, are reduced to avoid complex coupling with flapping behavior. The control objectives are: 1) the controller should stabilize the origin from non-zero initial conditions and 2) reject unknown disturbances. A control law is then proposed that stabilizes the origin under unknown disturbances using a sliding mode approach. A sliding surface is first defined, then a Lyapunov function, $V(s)$, proves that, in conjunction with an observer to estimate the disturbance, the controller successfully stabilizes the system. The observer makes use of previous literature to demonstrate convergence in finite time by framing the error under an advantageous form. Finally, numerical simulations with parameters of a typical fruit fly corroborate the analysis. An analysis of the numerical results are discussed in conjunction with the nonlinear control proofs.**

***Index Terms*—MAV, Flapping Vehicles, Sliding Mode Control, Nonlinear Control, Control Design, Observer Design**

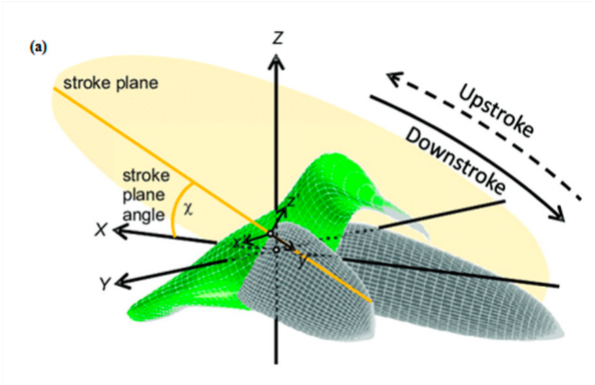

Fig. 1. MAVs typically studied in the literature include hummingbirds and insects. Pictured here is the stroke plane, a common control surface in MAVs, on a hummingbird [6]. These vehicles exert control by changing the stroke angle subtended by a wing, stroke plane angle, and wing angle

I. Introduction

Small natural fliers (or micro-aerial vehicles), like insects and small avian, have long fascinated researchers with their impressive maneuverability, stability, and ability to quickly transition between different flight conditions [1]. Such flight characteristics are are uniquely beneficial in reconnaissance for search and rescue, surveillance of risky or hazardous situations, remote inspection in civilian applications, or small-scale delivery systems [2]. While the potential applications are numerous and continue to grow, the construction, dynamic modelling, and control of such systems remains an active area of research. Specifically in attempting to control such vehicles, various linear and nonlinear approaches have been attempted. Early research began with linear PD control of roll-pitch-yaw using a time-averaged flapping model [3], while more current research has moved towards using sliding mode control for fully time-averaged nonlinear models [5], integrator backstepping for more complex aerodynamic models, and sliding mode control for partially linearized constructs [4]. In particular, this work focuses on attitude stabilization of a partially linearized model, building largely from the results presented in [4].

This work seeks to stabilize a flapping-wing, micro-aerial vehicle (MAV) using sliding mode control with the following control objectives:

- The controller should stabilize the system from non-zero initial conditions.
- The controller should reject unknown external disturbances.
- The controller may estimate the disturbance using an observer with finite-time convergence.

The resulting controller may find application as an inner-loop control for more complex trajectory tracking or maneurvering with an outer-loop controller.

II. Governing Dynamics

While MAV dynamic models become increasing sophisticated and accurate, a common nonlinear model derives the equations of motion in the body frame using a cycle-averaging technique. In cycle-averaging, moments and forces exerted on the body are time-averaged over one period using Floquent Theory [5]. As an example, the equation of one degree-of-freedom and a cycle-averaged moment are reproduced from [5]; the reader is refered to [5] for complete equations.

$$\ddot{\phi} = \frac{M_a x}{I_x} + \frac{M_a y}{I_y}(\sin\phi\tan\theta) + \frac{M_a z}{I_z}(\cos\phi\tan\theta) + \frac{I_y - I_z}{I_x}(qr) + \frac{I_z - I_x}{I_y}(pr\sin\phi\tan\theta) + \frac{I_x - I_y}{I_x}(pq\cos\phi\tan\theta) + \dot{\phi}\dot{\theta}\tan\theta + \dot{\theta}\dot{\psi}\sec\theta \quad (1)$$

$$\ldots$$

$$M_{ax} = G_1[\cos(\mu_L)(1+\delta_L)^2 - \cos(\mu_R)(1+\delta_R)^2] + (C_I y_{com}\cos(\beta) + \pi^2 y_H) \quad (2)$$

$$\ldots$$

where μ, β, δ are wing control surface inputs. While these dynamics represent a more complete expression of the system, this work is only considering attitude control for an inner-loop system, and thus, the partially-linearized dynamics found in [4] are more appropriate.

Ref. [4] builds on results presented in [7], which used system identification techniques to build a dynamic model of a typical fruit fly with three degrees of freedom as it hovers and engages in some maneuvering. The complete dynamics around a hovering conditions to be controlled in this work are:

$$\begin{bmatrix}\dot{\psi}_R\\ \dot{\psi}_P\\ \dot{\psi}_Y\end{bmatrix} = \begin{bmatrix}1 & \sin\phi_R\tan\phi_P & \cos\phi_R\tan\phi_P\\ 0 & \cos\phi_R & -\sin\phi_R\\ 0 & \sin\phi_R\sec\phi_P & \cos\phi_R\sec\phi_P\end{bmatrix}\begin{bmatrix}\omega_R\\ \omega_P\\ \omega_Y\end{bmatrix} \quad (3)$$

$$\dot{\omega} = A\omega + Bu + d(t) \quad (4)$$

where ψ_i represent the roll, pitch, and yaw body angles, ω_i represents the respective angle rates, $d(t)$ represents an unknown disturbance acting on the body frame, and A and B are matrices defined below. Note that the notation $T(\psi)$ will be used throughout to denote the matrix $\dot{\psi} = T(\psi)\omega$ for convenience.

$$A = \begin{bmatrix}C_4 L_p & 0 & C_1 N_r\\ 0 & C_3 M_q & 0\\ C_1 L_p & 0 & C_2 N_r\end{bmatrix} \quad (5)$$

$$B = \begin{bmatrix}C_4 L_{\Delta\Phi} & C_1 N_{\Delta\beta} & 0\\ 0 & 0 & C_3 M_{\bar{\Phi}}\\ C_4 L_{\Delta\Phi} & C_1 N_{\Delta\beta} & 0\end{bmatrix} \quad (6)$$

where

$$C_1 = \frac{I_{xz}}{I_{xx}I_{zz} - I_{xy}^2},\quad C_2 = \frac{I_{xx}}{I_{xx}I_{zz} - I_{xz}^2}$$
$$C_3 = \frac{1}{I_{yy}},\qquad C_4 = \frac{I_{zz}}{I_{xx}I_{zz} - I_{xz}^2} \quad (7)$$

Numerical values are populated for a common fruit fly in section IV. Coefficients L, M and N in A represent stability derivatives and, in B, represent control derivatives resulting from partial linearization about a hovering condition. Finally, the control inputs are perturbations to wing flapping characteristics: $u = [\Delta\Phi, \bar{\Phi}, \Delta\beta]$. Fig. 7 visualizes how the input commands change the flapping associated with a hovering condition. Finally, by establishing $x = [\psi; \omega]^T$ as the state-space, the system in (3) and (4) compose the nonlinear state space to be controlled.

III. Controller and Observer Design

A. Exponential Convergence Control Law

The first step in constructing a control law is to define a sliding surface that exhibits favorable dynamics. The goal of the control law is to then force the system towards the sliding surface and maintain motion along the surface. Using the natural split in dynamics, vectors ϕ and ω are used to construct s. The derivative is then taken and terms from (3) and (4) are directly substituted.

$$s = \omega + G\psi \quad (8)$$

$$\dot{s} = (A\omega + Bu + d(t)) + GT(\psi)\omega \quad (9)$$

where $s = [s_1, s_2, s_3]^T$ and G is a diagonal matrix of positive constants. When defined as such, a trajectory lying on the sliding surface will exponentially converge to the origin, stabilizing the MAV's attitude. To prove exponential convergence, a Lyapunov function is considered and differentiated with respect to time. The following choice is positive definite, radially unbound with respect to s, and $V(0) = 0$.

$$V(s) = \frac{1}{2}s^T s \quad (10)$$

$$\dot{V}(s) = s[(A\omega + Bu + d(t)) + GT(\psi)\omega] \quad (11)$$

From the Barbashin-Krasovskii theorem [9], the origin will be globally asymptotically convergent iff $\dot{V}(s) < 0 \ \ \forall s \neq 0$. While it is trivial to see V(s) is radially unbound, this section will focus on proving the $\dot{V}(s) < 0$ condition.

Consider the following input:

$$u = -B^{-1}\left[(A + GT(\psi))\,\omega + \hat{d} + \kappa_1 s + \kappa_2 \text{sgn}(s)\right] \quad (12)$$

where κ_1, κ_2 are positive. Substitution into (11) cancels the A, B, and T dependencies and yields:

$$\dot{V}(s) = -\kappa_1 s^T s - \kappa_2|s| - s^T(d(t) - \hat{d(t)}) \quad (13)$$

$$\dot{V}(s) = -\kappa_1 s^T s - |s|\kappa_2 - s^T e(t) \quad (14)$$

Inspection of terms one and two on the R.H.S are clearly negative, definite. The third term, however, is not necessarily negative, definite. Let's first assume a few conditions: 1) if the error is zero (i.e. there are no disturbances), then clearly the system is negative, definite for all s. Under no disturbances, the system will exponentially converge to the origin. 2) if the

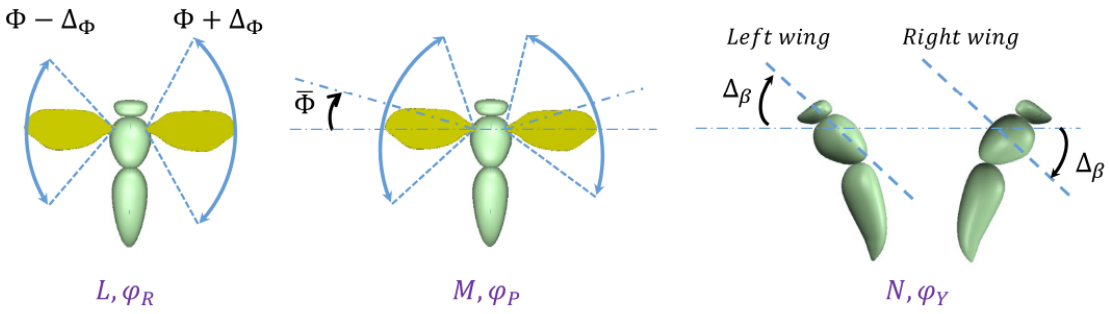

Fig. 2. Control inputs to a partially linearized model. The inputs act in the body orientation by changing the wing flapping characteristics, including stroke and stroke plane angle [7].

error is bound, then the following inequality is written (as demonstrated in [4]):

$$\dot{V}(s) \leq -\kappa_1 s^T s + |s||e(t)| \leq -\kappa_1 s^T s + 0.5(|s|^2 + |e_m|^2) \quad (15)$$

$$\dot{V}(s) \leq -(2\kappa_1 - 1)V + 0.5|e_m|^2 \quad (16)$$

where e_m is the maximum, bounded error over a finite time. Therefore, the signals are at least bounded during the transient period of the observer s.t. $\kappa_1 > 1/2$ [4]. Finally consider a third condition: 3) the restrictions are loosened by first assuming $|e(t)| \leq |d(t)|$. The Lyapunov function in (18) then reduces to:

$$\dot{V}(s) \leq -\kappa_1 s^T s - |s|(\kappa_2 - |d(t)|) \quad (17)$$

Which is negative, definite if $\kappa_2 > |d(t)|$. If the disturbance can be estimated *a priori*, then κ_2 can be appropriately selected to ensure exponential convergence (where C is a positive constant) [9]:

$$\dot{V}(s) \leq -\kappa_1 V - C\sqrt{V} \quad (18)$$

This constraint is realistic if a designer can design the controller for a general operating environment (e.g. outdoor vs. indoor wind gusts, which may be estimated). The only remaining proof is that the error must be bounded by the disturbance and the error shrinks to zero in finite time.

B. Finite-Time Observer

This section will exploit the results of [10] and [11] to build a finite-time observer; only results applicable to this problem will be detailed. First remark the following notation:

$$\lfloor \sigma \rceil^\nu = [|\sigma_1|^\nu \text{sgn}(\sigma_1), ..., |\sigma_n|^\nu \text{sgn}(\sigma_n)]^T \quad (19)$$

For this particular system, the observer can estimate the lumped disturbance with the following form from [11]:

$$\dot{\hat{\omega}} = -\lambda_0 L^{1/3} \lfloor \hat{\omega} - \omega \rceil^{2/3} + A\omega + Bu + \hat{d} \quad (20)$$

$$\dot{\hat{d}} = -\lambda_1 L^{2/3} \lfloor \hat{\omega} - \omega \rceil^{1/3} + \ddot{\hat{d}} \quad (21)$$

$$\dddot{\hat{d}} = -\lambda_2 L^0 \lfloor \hat{\omega} - \omega \rceil^0 \quad (22)$$

where $L^{[i]} = [L_0^i, L_1^i, L_2^i]$ and λ_n are all positive constants. Now, the goal of the disturbance observer is to estimate the error, thus the following definitions are introduced: $e_0 = \hat{\omega} - \omega, e_1 = \hat{d} - d, e_2 = \dot{\hat{d}} - \dot{d}$. Using system dynamics in 4, the angular acceleration terms of (20) will cancel, resulting in the following form:

$$\dot{e_0} = -\lambda_0 L^{[1/3]} \lfloor e_0 \rceil^{2/3} + e_1 \quad (23)$$

$$\dot{e_1} = -\lambda_1 L^{[2/3]} \lfloor e_0 \rceil^{1/3} + e_2 \quad (24)$$

$$\dot{e_2} = -\lambda_2 L^{[0]} \lfloor e_0 \rceil^0 \quad (25)$$

According to [11], a selection of positive constants for L will ensure finite-time stability of the error to the origin and that $|e(t)| < |d(t)|$. Therefore, the observer will converge to zero in finite time, satisfying the enforced conditions on the control law.

C. Control Analysis Conclusions

The presented analysis has reached the following conclusions. Sec. IV will demonstrate these with a numerical simulation.

1) Under zero disturbance, controller will exponentially stabilize the origin per thrm. 4.14 [9].
2) Under a disturbance, the signal, s, is bounded during the transient period of the observer.
3) The controller will at least exponentially stabilize the origin for all signals and disturbances if $\kappa_2 > |d(t)|$ and $|e(t)| \leq |d(t)|$ per thrm. 4.10 [9].

IV. Simulation and Discussion

A. Simulation Parameters and Design

As a demonstration, this control law is applied to the MAV dynamics of (3) and (4). To simulate the control of a MAV, the results from a hovering condition presented in [7] are adapted to the model presented here.

$$A = \begin{bmatrix} -15.2 & 0 & -19.31 \\ 0 & -2.61 & 0 \\ -8.13 & 0 & -43.2 \end{bmatrix}$$
$$B = \begin{bmatrix} 4275.5 & 2860.6 & 0 \\ 0 & 0 & 3590.7 \\ 2288.5 & 6397.4 & 0 \end{bmatrix} \quad (26)$$

Control law parameters are defined using parameters from [4] that satisfy the constraints presented in Sec. III. These, along with the nominal hovering condition parameters, are summarized in table I. The entire control law and observer are then built in SimuLink [8] and processed in MATLAB. The simulations are run using `ode45`, a 4th and 5th order Runge-Kutta integrator with adaptive time-stepping. See the appendix for the final SimuLink construction.

TABLE I
SIMULATION PARAMETERS

Parameter	Value	Description
L	$[1000, 1000, 1000]^T$	Observer constants
λ	1.1, $1.5\sqrt{3}$, 3	Observer constants
G	$20I_{3x3}$	Sliding surface constants
k_1, k_2	20, 1000	Lyapunov constants
ν	0.8	Observer constant
ϵ	0.5	Saturation limit
Φ_0	120^o	Nominal stroke angle
f	60	Nominal flapping freq. [Hz]

This simulation is divided into three parts: an initial stabilization from a non-zero a response to a constant, non-zero disturbance, and a response to a time-varying disturbance. To model this, the disturbance acting on (4) is written and simulated as:

$$d(t) = \begin{cases} 0 & \text{if } 0 \leq t < 5 \\ [300, -300, 150]^T \text{ mN} & \text{if } 5 \leq t < 10 \\ 20[3\sin(3\pi t) + 2, 0.2\sin(2\pi t) - 1, & \\ 0.5\sin(t) + 1]^T + N \text{ mN} & \text{if } 10 \leq t < 20 \end{cases} \quad (27)$$

where N is injected white noise. Finally, the system is simulated with the input as written. As expected, this controller suffers from chattering as the inputs quickly switch between the sgn(s). To correct, a new input is defined substituting the sgn(s) with sat(s); see (28). Without loss of generality, the Lyapunov analysis of the controller holds for sat(s) as well as sgn(s), and and previous conclusions on stability are still valid [9]. The simulation is then repeatably run where the saturation limit, ϵ, is increased until the chattering clears (around 0.5). Some ramifications of this substitution are discussed later.

$$u = -B^{-1}\left[(A + GT(\psi))\,\omega + \hat{d} + \kappa_1 s + \kappa_2 \text{sat}(s/\epsilon)\right] \quad (28)$$

B. Non-zero Initial Condition and Disturbance Response

The simulation is initialized with Euler angles $\phi(0) = [10, 5, 15]^T$, angular rates $\omega(0) = 0$, and observer initial conditions $e(0) = 0$. The response under the designed law is in Fig. 3. Without an external disturbance and full knowledge of the states, the MAV quickly stabilizes to the origin in agreement with the Lyapunov analysis along the sliding surface.

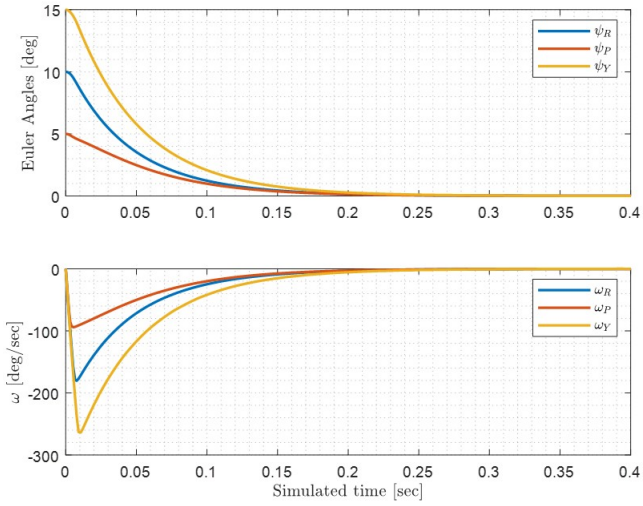

Fig. 3. Simulation of the MAV system to a non-zero initial condition without any external disturbances. Angles represent Euler angles in the body reference frame

Per conclusion 1) from Sec. III.C, the controller does stabilize the origin from a non-zero initial condition. Continuing the simulation, after five seconds, a constant external disturbance, followed by a time-varying disturbance, acts on the system. By judiciously selecting the constant κ_2 to exceed the L1 norm of the disturbance, the analysis suggests a convergent system. The simulation is run with the constant disturbance for 5 seconds and the time-varying for 10 seconds; Fig. 4 shows the observer's recreation of the disturbance and Fig. 5 plots the Euler angle response.

The disturbance was successfully recreated in the step case. As a consequence of the successful recreation, the controller may converge to the origin as the estimation error shrinks to zero in finite time as simulated in Fig. 5. Both Sec III.C conclusions 2) and 3) are successfully demonstrated under this test. Past 10 seconds, the time-varying disturbances amplitudes were appropriately recreated but with a small phase-lag. This lag causes a small error in to persist, and therefore, the MAV never fully converges to zero. In Fig. 5 at t $>$ 11.5 sec, some small oscillations exist in the states.

C. Control Effort and Flapping Behavior

To avoid complex phenomena and modelling associated with flapping behavior, this problem exploits a partially linearized model. Thus, the control efforts are described as perturbations to the position and dynamics of the left and right wings (see Fig. 2). Fig. 6 visualizes the input history for the

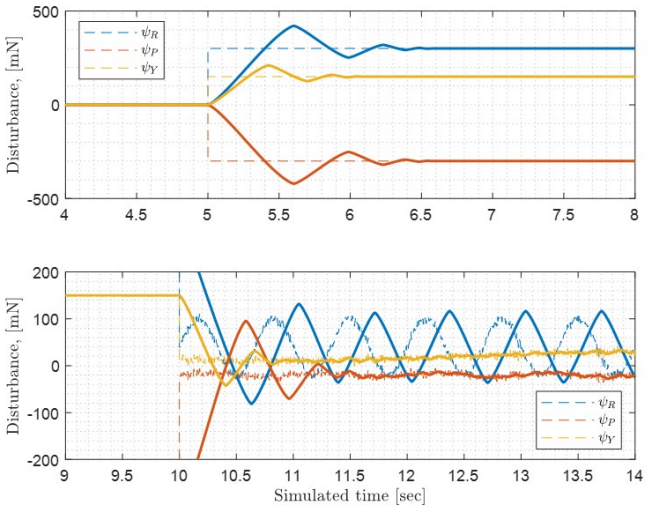

Fig. 4. The observer's disturbance estimate for a step response at $5 \leq t < 10$ and a time-varying response at $10 \leq t < 20$. The dotted lines indicate exact commanded disturbances while the solid lines show the recreation

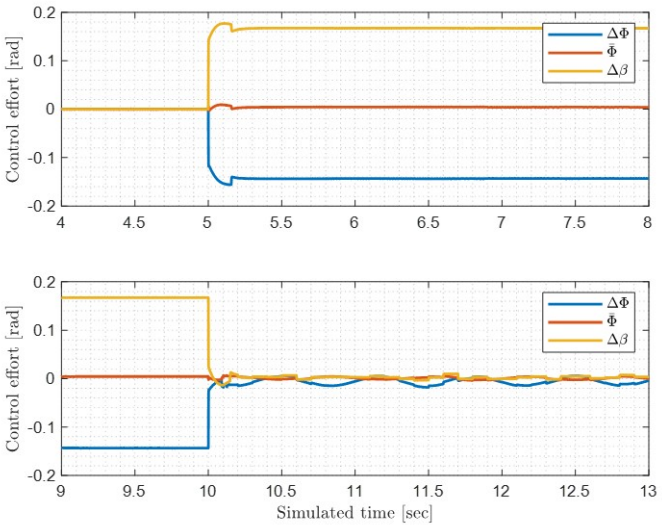

Fig. 6. Control effort (represented as perturbations to wing position amongst a hovering flight) as different disturbances are exerted on the MAV. The control appears to closely follow the disturbance profile.

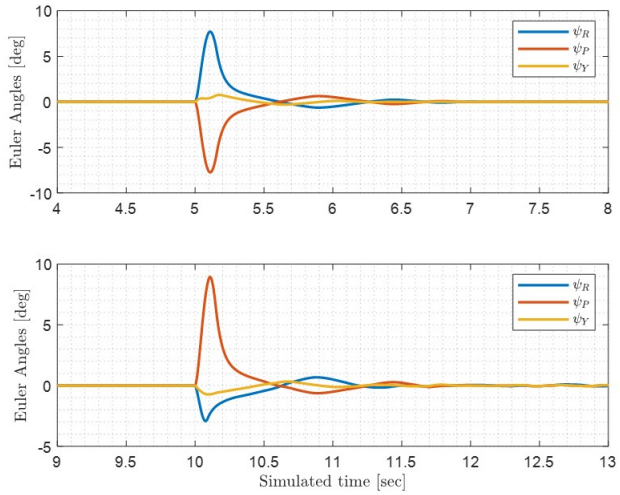

Fig. 5. The MAV's response to the injected disturbances. The change in disturbance from zero to step then to time-varying show marked jumps, but quick convergence back to zero (or close to zero).

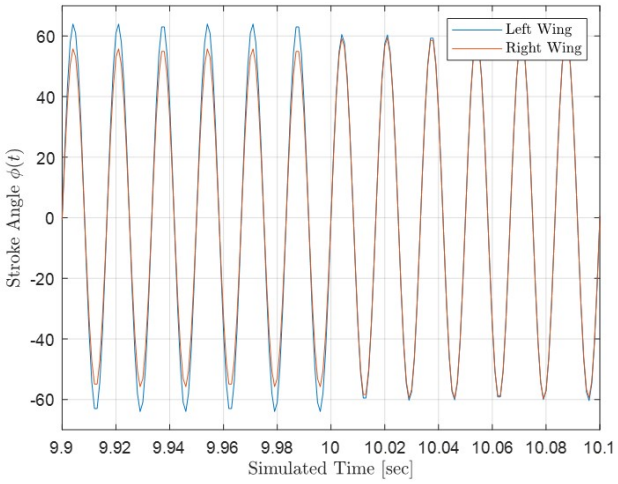

Fig. 7. Stroke angles about a hovering condition with inputs from the controller. Before the step change in disturbance, the left and right wings are slightly mis-matched in amplitude to compensate for the disturbance.

stabilization around the disturbances at $t = 5$ and $t = 10$. The step-like behavior is in correction to the constant disturbances acting in the MAV's body frame, while the oscillations at $t > 10$ are dynamic reactions to correcting the time-varying disturbance. To physically relate this to hovering stabilization, Fig. 7 shows how input $\Delta\Phi$ modifies the flapping behavior around a hovering condition. The step disturbance at $t < 10$, for example, shows the left wing exerting greater effort to stabilize in the presence of the disturbance. At $t > 10$, the left and right wing follow begin to follow similar stroke patterns as the large disturbance is replaced with a smaller, oscillating one.

D. Sliding-Mode Analysis

This control law ultimately functions by pushing the dynamics to, and holding along, the sliding surface defined by (8). Under a two-state system enforced with a sliding mode law, a trajectory will encircle the phase portrait until reaching the sliding surface when it then converges to the origin. While this system contains six states, the natural division between Euler angles and velocities lends itself well to creating a similar plot.

Fig. 8 uses a sgn(s) function and an L1 norm to visualize a portrait of the trajectory's history (note that sgn(s) takes the most prevalent sign amongst $[s_1, s_2, s_3]$ to agree with the dimensions of the portrait). Starting at t = 0, the controller

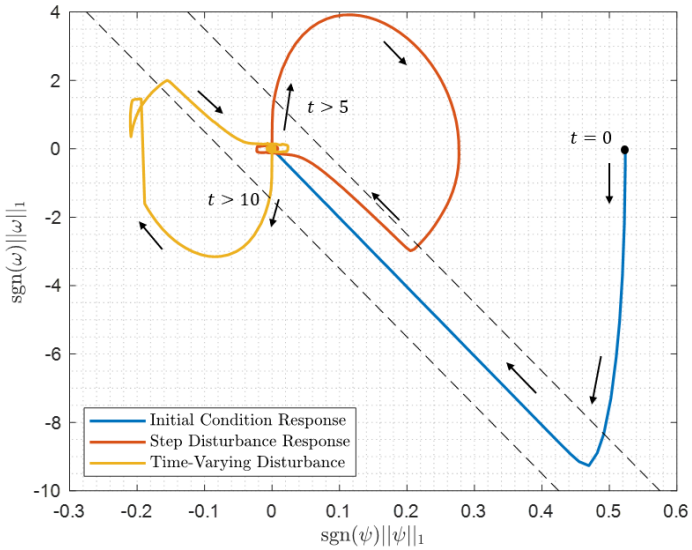

Fig. 8. A phase-portrait style plot of the trajectory's history. The controller enforces the desired sliding surface within an approximated boundary layer, shown in black dashed lines. All trajectories converge to a region of attraction close to the origin. Arrows indicate the progression of time.

immediately pushes the dynamics towards the sliding surface. Perturbations at t = 5 and t = 10 push the system off the region of attraction, but the controller successfully returns the trajectory back towards the sliding surface. Note in Fig. 8 that a boundary layer around the sliding surface exists from the modification made to the controller to avoid chattering. The dotted lines indicate $\pm 3\epsilon$ to agree with the L1 norm.

V. Conclusions

This work successfully stabilized a MAV using sliding mode control. By defining the sliding mode as $s = \omega + G\phi$, an input was judiciously selected to prove convergence, for any s, assuming no input disturbance. Then, using a finite-time observer to estimate the disturbance, it was then proved that the controller could stabilize the system such that the designer had some knowledge of the operating environment *a priori*. A numerical solution then showed 1) the controller successfully converged to the origin under non-zero initial conditions and a constant disturbance and 2) the controller stabilized the system under a time-varying disturbance. Similarly, the results show the observer accurately estimating the disturbance under constant conditions, and estimating with a small lag in time-varying conditions. Finally, an analysis of ω vs ϕ shows the sliding mode controller is functioning as expected.

As indicated in the introduction, this controller may find application as an inner-loop controller. Future research may make use of these results and perform reference tracking in an outer-loop or to perform more complicated maneuvering. Another direction for future research may include relaxing the hovering condition and creating a more general sliding mode nonlinear controller.

VI. Appendix

Fig 9 shows the input to the simulation where the input makes use of a sgn(s) rather than a sat(s). The physical inputs would be changes to wing positioning and flapping, thus, the chattering would be nearly physically impossible to realize. The sgn(s) shows clear chattering as the input jumps between $\pm s$. By introducing sat(s) in place of sgn(s) and tuning the saturation point, the controller largely eliminated the chattering.

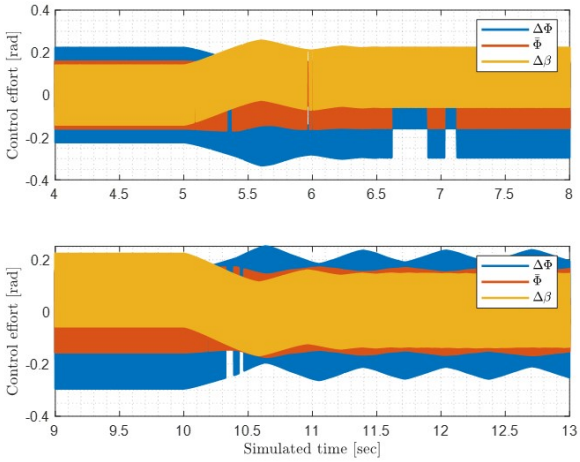

Fig. 9. sgn(s) causes chattering in the input that is avoided by tuning a sat(s) in its place in the controller

Fig 10 (next page) shows the SimuLink construction used to solve the system of equations described throughout.

References

[1] R. Dudley, The biomechanics of insect flight: form, function, evolution, Princeton University Press, 2002.

[2] Khan, Q.; Akmeliawati, R. Review on System Identification and Mathematical Modeling of Flapping Wing Micro-Aerial Vehicles. Appl. Sci. 2021, 11, 1546. https://doi.org/10.3390/app11041546

[3] Zhang, X., Liu, H.: A three-axis pd control model for bumblebee hovering stabilization. J. Bionic Eng. 15(3), 494–504 (2018)

[4] X. Tran, H. Oh, I. Kim, S. Kim, Attitude stabilization of flapping micro-air vehicles via an observer-based sliding mode control method. Aerospace Science and Technology 76, 386-393, (2018).

[5] B. Wissa, K. Elshafei, A. El-Badawy, Lyapunov-based control and trajectory tracking of a 6-DOF flapping wing micro aerial vehicle, Jour. Nonlinear Control 99, 2919–2938, (2020). https://doi.org/10.1007/s11071-020-05487-9

[6] Knowles, K.; Phillips, N. Reynolds number and stroke amplitude effects on the leading-edge vortex on an insect-like flapping wing. In Proceedings of the International Powered Lift Conference, Philadelphia, PA, USA, 5–7 October 2010.

[7] B. Cheng, X. Deng, Near-hover dynamics and attitude stabilization of an insect model, in: Proc. 2010 Am. Control Conf, 2010, pp. 39–44.

[8] The MathWorks, Inc. (2024)

[9] H. K. Khalil, "Nonlinear Systems," 3rd Edition, Prentice Hall, Upper Saddle River, 2002.

[10] Y.B. Shtessel, I.A. Shkolnikov, A. Levant, Smooth second-order sliding modes: missile guidance application, Automatica 43 (2007) 1470–1476.

[11] A. Levant, M. Livne, Exact differentiation of signals with unbounded higher derivatives, IEEE Trans. Autom. Control 57 (2012) 1076–1080.

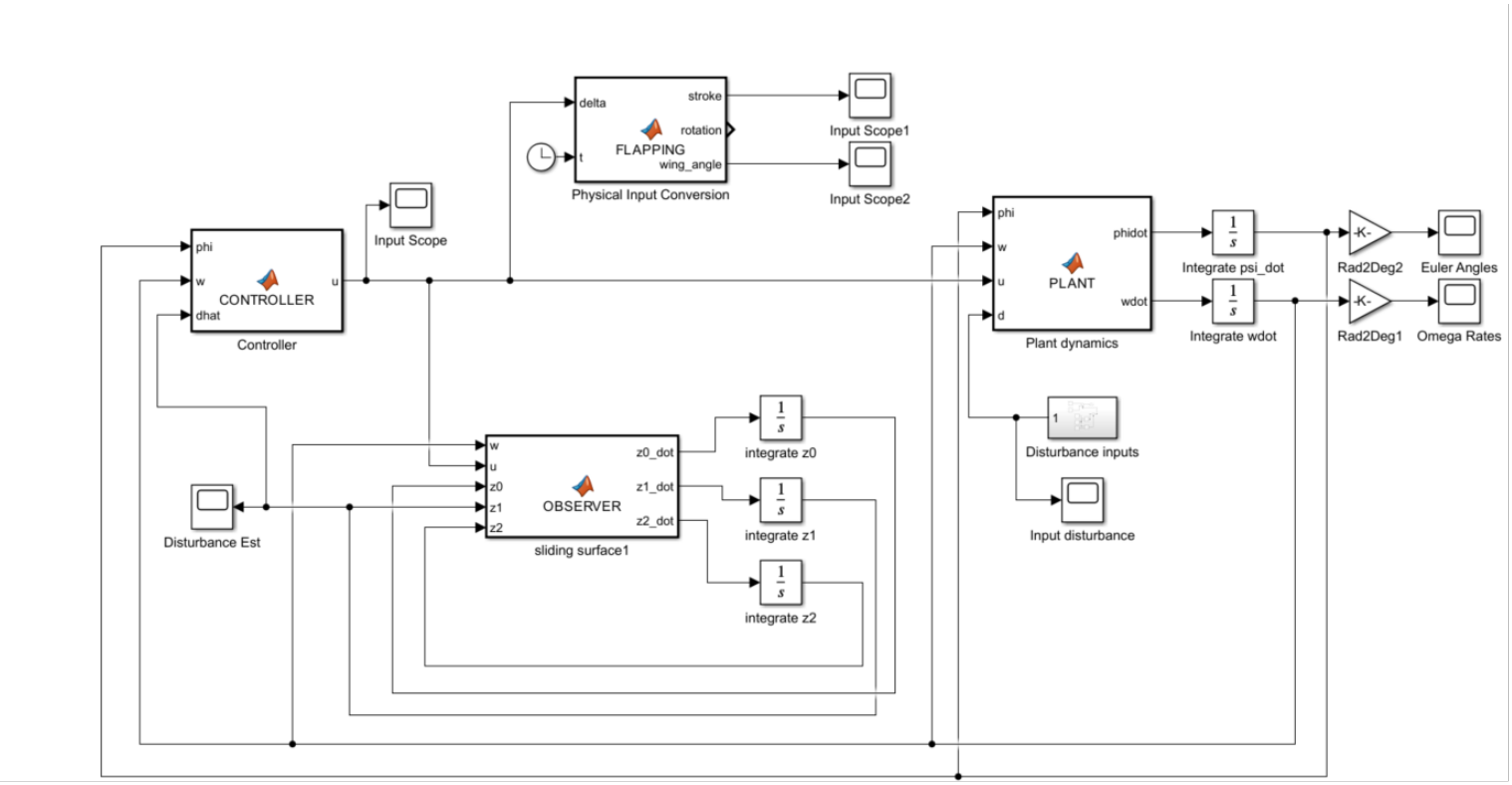

Fig. 10. The SimuLink model built was used to model the plant, observer, and controller equations. SimuLink makes use of a RK-4 and RK-5 numerical scheme with adaptive time stepping to solve the equations.